Radiative Heat Transfer Analysis of Fibrous Insulation Materials Using the Zonal–GEF Method

Walter W. Yuen*

University of California at Santa Barbara, Santa Barbara, California 93106

and

George Cunnington†

Cunnington and Associates, Palo Alto, California 94303

The zonal method, together with the concept of generic exchange factor, is shown to be an efficient and accurate approach to analyze radiative heat transfer in high porosity insulation materials which have a large scattering coefficient. Numerical predictions generated by the method correlate well with experimental data generated for LI900, a material used in the insulation tile for the space shuttle. Comparisons are presented for measurement in emitted surface intensity, effective thermal conductivity, and thermal response under radiant heating. The heat transfer characteristics for the material are also determined. For LI900 which is effectively a pure scattering material at the short wavelength region ($\lambda < 5 \ \mu$m), radiation from high temperature sources can be transmitted through the material even when the optical thickness is large. Radiative heat transfer in this class of material is nonlocalized in the optically thick limit. A nonlocalized radiation model such as the zonal–generic exchange factor method is needed to determine the thermal behavior of the material for design purposes.

Nomenclature

D_L = distance between volume element V_1 and the lower wall, Fig. 1
D_m = distance between the two volume element V_1 and V_2, Fig. 1
D_{tot} = distance between volume element V_1 and the lower wall, Fig. 1
d = thickness of volume element, Fig. 1
f_v = volume fraction
$g_1 g_2$ = total exchange factor between volume element V_1 and volume element V_2
$g_1 g_{2,t}$ = spectrally integrated total exchange factor between volume element V_1 and volume element V_2
k_1 = average extinction coefficient in volume element V_1
k_2 = average extinction coefficient in volume element V_1
k_{eff} = effective thermal conductivity
k_L = average extinction coefficient in region between V_1 and the lower wall
k_m = average extinction coefficient in region between the two volume element V_1 and V_2
k_{tot} = average extinction coefficient in region between volume element V_1 and the lower wall
L = thickness of sample used in the effective thermal conductivity calculation
n = the number of intervening volume element in the exchange factors $s_1 g_1(n)$ and $g_1 g_2(n)$
Q = heat flux
S_1 = the lower wall, Fig. 1
S_2 = the upper wall, Fig. 1
$s_1 g_1$ = total exchange factor between the lower wall and volume element V_1

$s_1 g_{1,t}$ = spectrally integrated total exchange factor between the lower wall and volume element V_1
$s_1 s_1$ = total exchange factor between the lower wall and itself
$s_1 s_{1,t}$ = spectrally integrated total exchange factor between the lower wall and itself
$s_1 s_2$ = total exchange factor between the lower wall and upper wall
$s_1 s_{2,t}$ = spectrally integrated total exchange factor between the lower wall and upper wall
T = temperature
x = coordinate used in the transient heating calculation
ΔT = temperature difference in the effective thermal conductivity calculation

I. Introduction

RADIATIVE heat transfer through highly porous fibrous composite materials is a problem of considerable practical interest because of the widespread use of fiber composites in many areas such as the development of thermal protection systems for the Space Shuttle Orbiter and other commercial insulation systems. But in spite of the significant improvement in the understanding of the physics of radiative transport through this class of material [1] and also the rapid increase in the available computational power, the common design practice used by the insulation designers remains quite primitive. For example, the concept of "effective thermal conductivity" appears to be still the most commonly used approach for design. Using standard apparatus such as the guarded-hot-plate, data for "effective thermal conductivity" are generated and standard conduction-only thermal analysis software packages are then used to verify the feasibility of a specific design.

A primary difficulty preventing engineers from using a more physically sophisticated and accurate design approach is the lack of an efficient and accurate computational tool for the assessment of radiative heat transfer. Although a great deal of work has been reported over the past 20 years on various computational techniques for radiative heat transfer [2,3], most of these existing techniques are not sufficiently accurate, efficient, and suitable for use by nonradiation experts in design applications. The objective of this work is to show that the zonal method, together with the concept of generic exchange factor (GEF), is an accurate and efficient approach for the analysis of radiative heat transfer in high porosity fibrous composite materials. The GEF concept was originally developed for

*Professor, Department of Mechanical and Environmental Engineering, University of California at Santa Barbara. Senior Member AIAA.
†Associate Fellow AIAA.
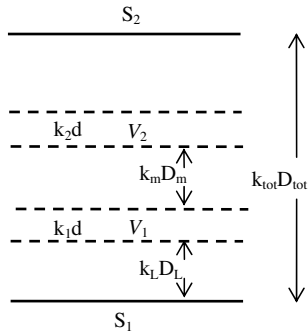
Fig. 1   Geometry of the two example volume elements in the parallel slab geometry.

application to nonscattering inhomogeneous and nonisothermal materials [4,5]. In this work, this concept is extended and shown to be effective for nonisothermal, homogeneous isotropically scattering medium. As shown in a previous work [6], the highly anisotropic scattering behavior of fibrous composites can be reformulated to an equivalent isotropically scattering medium using the approach developed by Joseph et al. [7]. The concept of GEF can thus be applied to analyze thermal behavior of general homogenous nonisothermal fibrous composite materials.

In Sec. II, the mathematical formulation of GEF for composites in a one-dimensional parallel slab geometry is presented. A two step procedure is used. First, fiber characteristics (optical properties, size distribution) and packing information (orientation, volume fraction) of the composite are used to generate the spectral absorption coefficient, extinction coefficient and scattering phase function using Mie theory [1]. The zonal method is then used to generate the GEF's. In Sec. III, the method is used to analyze the heat transfer characteristics of LI900 thermal insulation, which is a composite material consisting of 4.0 μm mean-diameter silica fibers packed with random orientation. This material is selected for analysis because fiber size distribution, together with experimental data on heat transfer and effective thermal conductivity were available [8]. The accuracy of the zonal–GEF method can thus be demonstrated by a direct comparison with experimental data. Heat transfer characteristics for this class of material are identified. Finally, some concluding remarks are presented in Sec. IV.

II.   The Zonal–GEF Method for an Absorbing Scattering Medium

The concept of "generic exchange factor (GEF)" has been developed and applied successfully to nonscattering media [4,5]. Physically, the GEF concept is based on the expectation that the radiative exchange between two volumes (or surfaces) should be only a function of the absorption coefficients (or emissivities) of the two volumes (or surfaces) and the absorption coefficient of the intervening medium. If GEF's are tabulated for basic computational elements (e.g., a cubical element) and covering the full range of optical dimensions, these factors can be used universally for all calculations, accounting for the effect of inhomogeneity and the transient evolution of the properties (e.g., temperature, pressure, density) of the medium.

For a scattering medium, however, the applicability of the GEF concept is questionable because the radiative exchange between two volumes in a scattering medium depends generally on the absorption and scattering characteristics of the whole computational domain. In a one-dimensional slab geometry as shown in Fig. 1, for example, the radiative exchange between the two volumes V_1 and V_2 depends not only on the absorption and scattering characteristics of the two volumes and the intervening medium, but also the absorption and scattering characteristics of the surrounding media (e.g., the optical thickness $k_L D_L$, $k_m D_m$, $k_{tot} D_{tot}$ and the associated scattering albedo). The total exchange factor calculated for the two volumes V_1 and V_2, for the same optical dimensions ($k_1 d$ and $k_2 d$) and intervening

optical thickness $k_m D_m$, can have different values for slabs with different total optical thickness $k_{tot} D_{tot}$.

A detailed consideration of numerical behavior of the total exchange factor, however, shows that for a homogeneous slab with constant extinction coefficient and scattering albedo, the effect of the overall geometry on the total exchange factors is generally small. For example, the total exchange factor between the lower wall S_1 and the volume V_1, $s_1 g_1$, is a function primarily of the optical thickness of the volume V_1, $k_1 d$ and the optical thickness of the intervening medium, $k_L D_L$. The effect of other optical thicknesses on the total exchange factor is quite weak. For a volume element that is optically transparent to the lower wall ($k_L D_L = 0$), numerical data for $s_1 g_1$ generated with a one zone calculation ($k_{tot} D_{tot} = k_1 d$, the volume V_1 is the total volume) and a two-zone calculation ($k_{tot} D_{tot} = 2 k_1 d$, the volume V_1 is separated from the top wall by a volume with equal optical thickness) are shown in Fig. 2a. Similarly, the exchange factor between the two volume elements with identical optical thicknesses ($k_1 d = k_2 d$), $g_1 g_2$, generated from a two-zone calculation ($k_{tot} D_{tot} = 2 k_1 d$, $k_L D_L = 0$, the two volumes V_1 and V_2 represent the total volume) and a three-zone calculation ($k_{tot} D_{tot} = 3 k_1 d$, $k_L D_L = 0$, the volume V_2 is separated from the top wall by a volume with equal optical thickness) are shown in Fig. 2b. It can be readily observed that the presence of an additional layer of materials with identical optical properties has essentially no effect on the two total exchange factors. Even though the numerical data

a)

b)
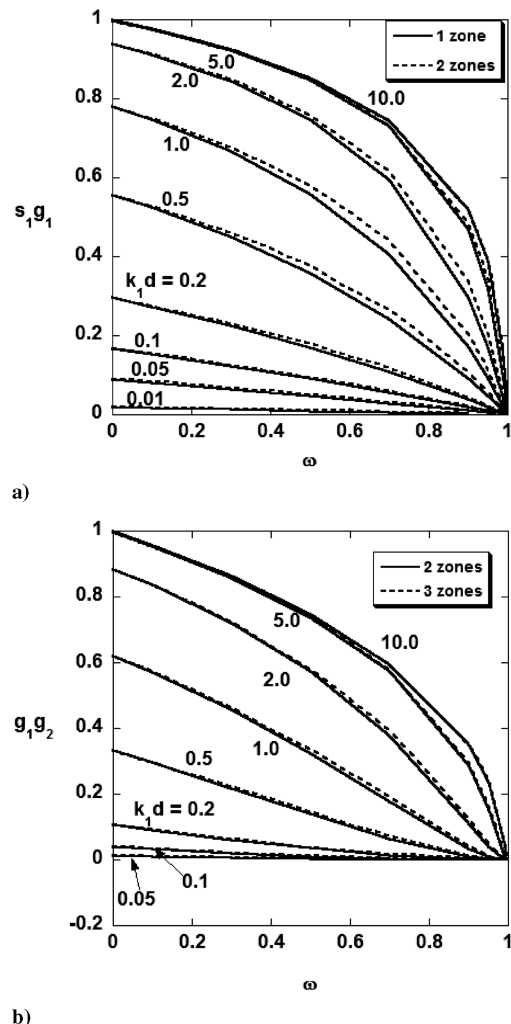
Fig. 2   a) The total exchange factor between V_1 and S_1 (with $k_L D_L = 0$) based on a 1-zone ($k_{tot} D_{tot} = k_1 d$) and 2-zones ($k_{tot} D_{tot} = 2 k_1 d$) calculation. ω is the scattering albedo. b) The total exchange factor between V_1, and V_2 (with $k_L D_L = 0$, $k_1 d = k_2 d$), based on a 2-zones ($k_{tot} D_{tot} = 2 k_1 d$) and 3-zones ($k_{tot} D_{tot} = 2 k_1 d$) calculation. ω is the scattering albedo.

presented are limited to the addition of one additional layer of materials, this general behavior is observed to be generally true and the total exchange factors are insensitive to optical properties of the surrounding. It is observed to be true also for exchange factors with a nonzero intervening optical thickness ($k_m D_m > 0$ and $k_L D_L > 0$). Physically, the total exchange factor $s_1 g_1$ can be interpreted as the apparent emissivity of a homogeneous absorbing, isotropically scattering slab. Results in Fig. 2a suggest that the slab's apparent emissivity is independent of the optical properties of any additional materials surrounding the slab.

For an absorbing and isotropically scattering parallel slab, a set of four GEF's can thus be defined and they can be applied universally to all radiative heat transfer calculations for the same geometry. Specifically, they are the two surface-to-surface exchange factors [$s_1 s_1(k_{tot} D_{tot})$ and $s_1 s_2(k_{tot} D_{tot})$] which are functions only of the total optical thickness of the slab, and the surface to volume exchange factor $s_1 g_1(k_1 d, k_L D_L)$, the volume to volume exchange factor $g_1 g_2(k_1 d, k_m D_m)$ which are functions of the optical properties of the volume element and the properties of the intervening medium. These factors can be readily tabulated accurately using the zonal method.

The mathematical behavior of the two surface-to-surface exchange factors is shown in Figs. 3 and 4. Physically, these two exchange factors, $s_1 s_1(k_{tot} D_{tot})$ and $s_1 s_2(k_{tot} D_{tot})$, are the hemispherical reflectivity and transmissivity of a homogeneous isotropically scattering slab, respectively. Results show that the reflectivity is generally small except for a high scattering ($\omega > 0.5$) medium with large optical thickness ($k_{tot} D_{tot} > 1.0$). The transmissivity decreases rapidly with increasing optical thickness except for a high scattering material ($\omega > 0.9$).

The mathematical behavior for $s_1 g_1(k_1 d, k_L D_L = 0)$ and $g_1 g_2(k_1 d, k_m D_m = 0)$ has already been presented in Figs. 2a and 2b. For a general finite difference calculation for a parallel slab with uniform grid size, the relevant optical dimensions for the two volume exchange factors are those with $k_L D_L = n k_1 d$ and $k_m D_m = n k_1 d$. Using the notation of $s_1 g_1(n) = s_1 g_1(k_1 d, n k_1 d)$ and $g_1 g_2(n) = g_1 g_2(k_1 d, n k_1 d)$, numerical data for $s_1 g_1(1)$ and $g_1 g_2(1)$ are shown in Figs. 5 and 6. Physically, these two exchange factors represent the radiative exchange between a volume (or surface) element with the first nonadjacent volume element (separated by one volume element of the same optical thickness). The magnitude of these factors thus represents the level of nonlocalized radiative interaction. It is interesting to note that these factors are nonzero and finite not only in the limit of small optical thickness ($k_1 d < 0.5$), but also in the optically thick condition ($k_1 d > 1.0$) when the scattering albedo is large ($\omega > 0.9$). The traditional approach to associate large optical thickness with localized radiative interaction is thus accurate only for nonscattering media. For media with a large scattering albedo, the
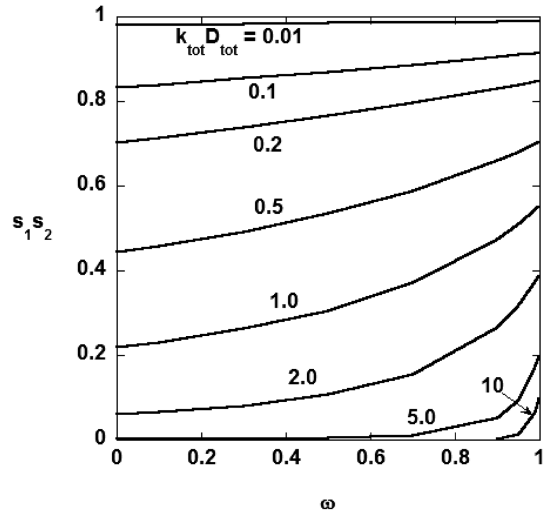

Fig. 4   The exchange factor $s_1 s_2$ for a one-dimensional parallel slab at different total optical thicknesses and scattering albedos.
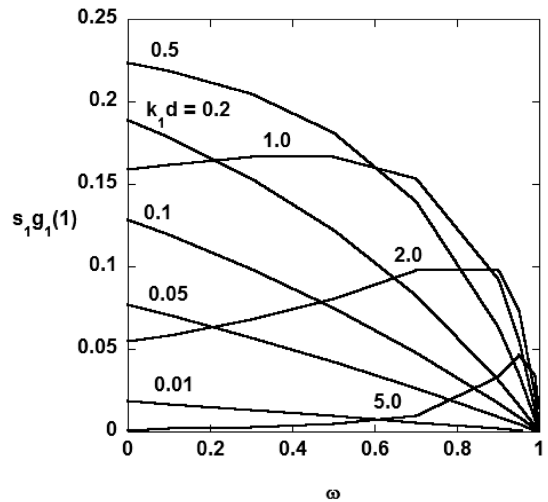

Fig. 5   The exchange factor $s_1 g_1(1)$ for a one-dimensional parallel slab at different optical thickness for the volume element V_1 and scattering albedo.
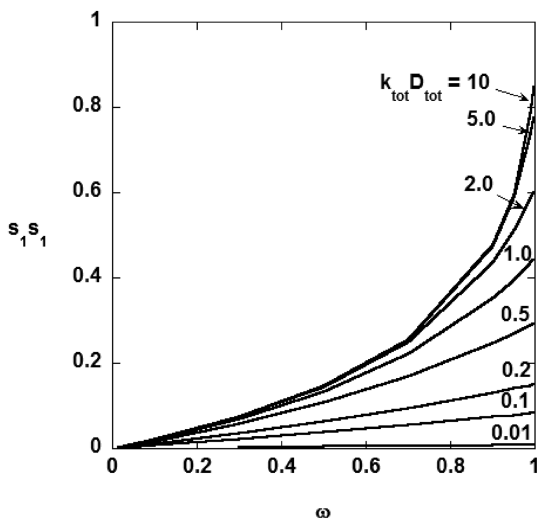

Fig. 3   The exchange factor $s_1 s_1$ for a one-dimensional parallel slab at different total optical thickness and scattering albedo.
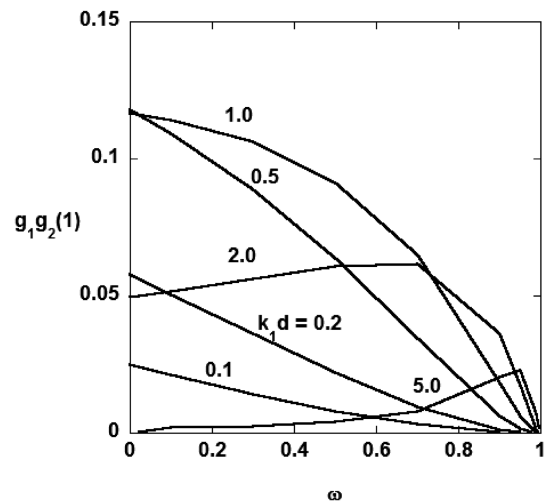

Fig. 6   The exchange factor $g_1 g_2(1)$ for a one-dimensional parallel slab at different optical thickness of the volume element V_1 and scattering albedo.

effect of nonlocalized radiative exchange cannot be neglected even in the optically thick region (e.g., $k_1 d > 1.0$).

Tabulated GEF's such as those presented in Figs. 2a, 2b, and 3–6, together with $s_1 g_1(n)$ and $g_1 g_2(n)$ with higher values of n, represent a complete set of exchange factors that can be used universally in the calculation of radiative heat transfer in any one-dimensional parallel slab with constant radiative properties.

III. Analysis of Radiative Heat Transfer of a LI900 Insulation Tile

The zonal–GEF method is applied to analyze the radiative heat transfer in a LI900 insulation tile. This material, which is a fibrous composite consisting of randomly packed nominally 4 μm diameter silica fibers, is selected because its optical properties, fiber size distribution, and packing orientation are well characterized and experimental data are available to verify the numerical calculations.

Specifically, using the measured index of refraction (n, κ) for silica fiber and assuming that the fibers are randomly packed, Mie theory is used to calculate the extinction coefficient, absorption coefficient, and anisotropically scattering factor, summing over the known fiber size distribution. The method of calculation has already been presented in [1,9]. Numerical data for material with a volume fraction of 0.0677 (at which the scattering by the fiber is in the independent scattering regime) are shown in Figs. 7a and 7b. Using the reformulation approach developed by Joseph et al. [7], the medium

can be treated as an equivalent isotropically scattering medium with the modified extinction coefficient as shown in Fig. 8 (the absorption coefficient, which remains unchanged, is shown in the figure for comparison). The detailed mathematics for this reformulation

Fig. 8 Modified absorption coefficient and extinction coefficient computed for the LI900 composite material with a fiber volume fraction of 0.0677 based on Mie theory.

Fig. 9 Measurements of spectral intensity of a LI900 slab with a surface temperature of approximately 1750 K.
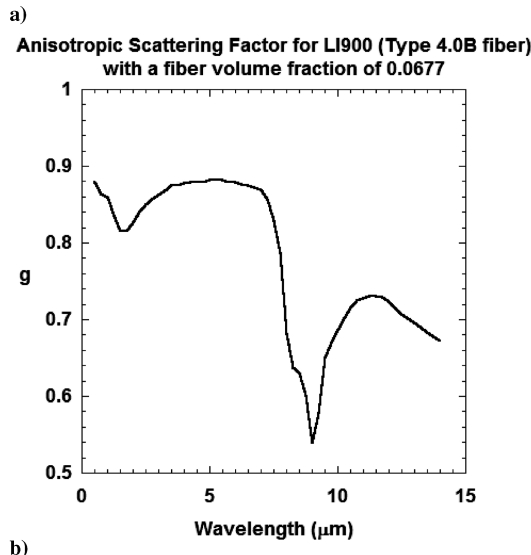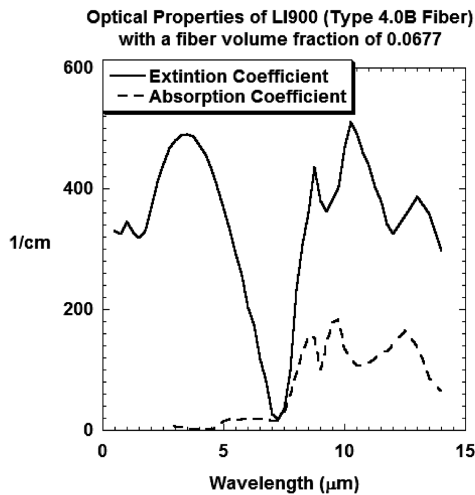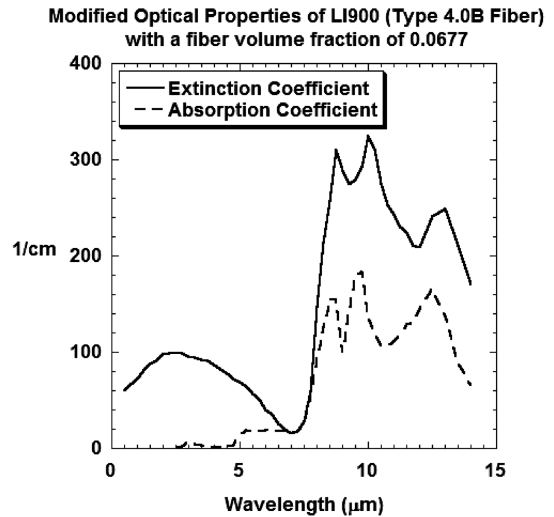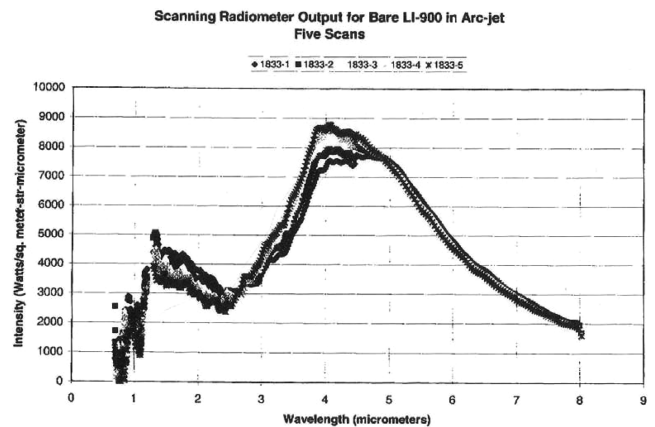
a)

b)

Fig. 7 a) Absorption coefficient and extinction coefficient computed for the LI900 composite material with a fiber volume fraction of 0.0677 based on Mie theory. b) Anisotropically scattering factor computed for the LI900 composite material based on Mie theory.
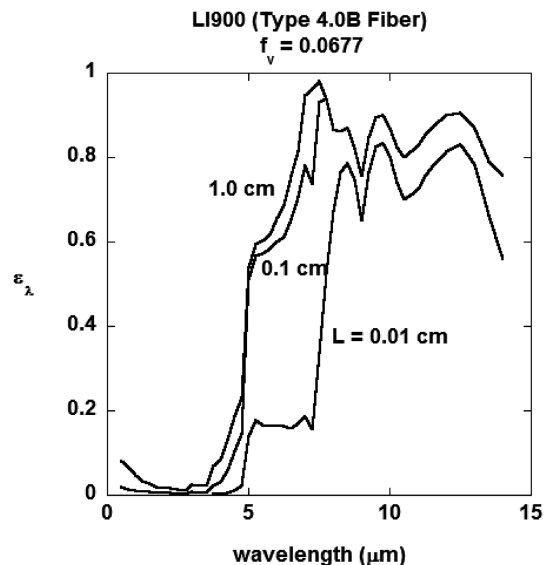
Fig. 10 Spectral emissivity of a LI900 slab with volume fraction of 0.0677 and various thicknesses.

process has been presented elsewhere [6] and is not repeated here. The optical properties as presented in Fig. 8, together with the tabulated GEF's, can be used to generate the integrated exchange factors needed for the heat transfer calculations. It is important to note that in the independent scattering regime, the absorption coefficient and extinction coefficient are directly proportional to the packing volume fraction. Data presented in Figs. 7a, 7b, and 8 can be applied to packing with other volume fraction by a multiplicative factor of $f_v/0.0677$.

Three sets of experimental data have been obtained for the LI900 composites with a fiber volume fraction of 0.0677. These data will be analyzed in the following three sections to demonstrate the heat transfer characteristics of this material and the feasibility of the zonal–GEF method.

A. Spectral Intensity

Measurements were made of the directional spectral intensity from a LI900 composite slab with a fiber volume fraction of 0.0677 heated convectively in an arc-plasma hypersonic wind tunnel. Typical data (Bouslog, S., private communication, October 2003)

LI900 (Type 4.0B Fiber)
$f_v = 0.0677$, L = 0.01cm

a)

LI900 (Type 4.0B Fiber)
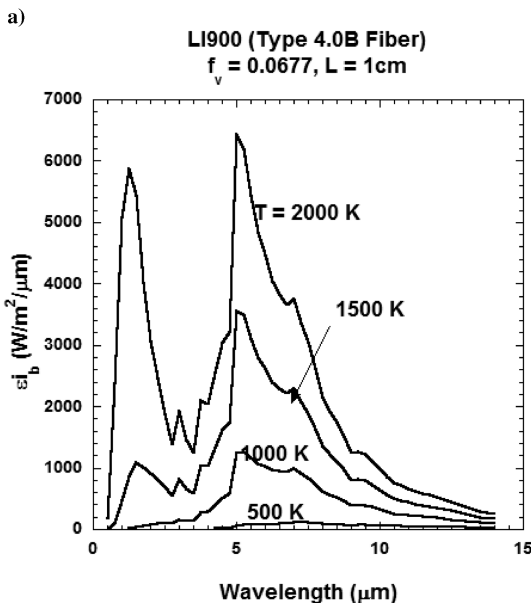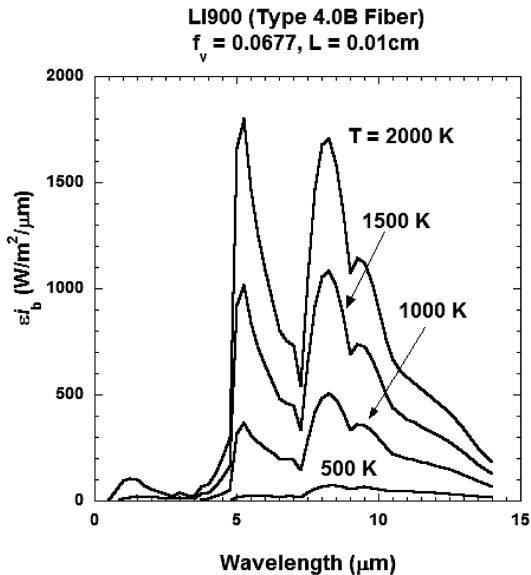**$f_v = 0.0677$, L = 1cm**

b)

Fig. 11 a) Spectral intensity radiated from a 0.01 cm thick LI900 slab with fiber volume fraction of 0.0677. b) Spectral intensity radiated from a 1 cm thick LI900 slab with fiber volume fraction of 0.0677.
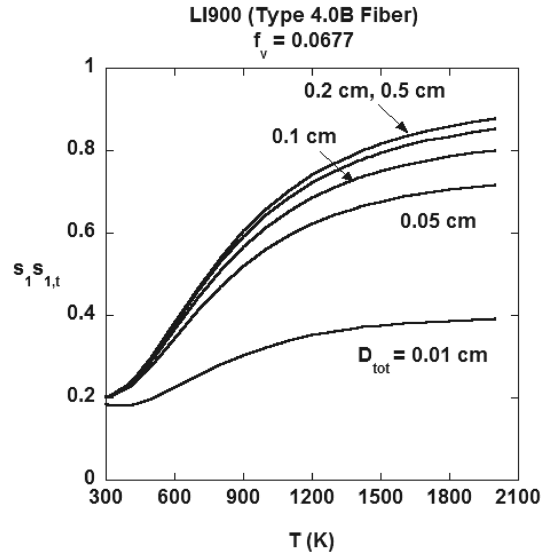
LI900 (Type 4.0B Fiber)
$f_v = 0.0677$

Fig. 12 The total exchange factor $s_1s_{1,t}$ as a function of temperature and total slab thickness.

are presented in Fig. 9. The convective heat flux was 16 W/cm^2 and at the time of the measurement, the surface was estimated to be at a temperature of 1750 K. No information was given as to the fiber size distribution and volume fraction of the test material. The thickness of the slab was 5 cm and its rear surface was attached to a water cooled plate.

Using the absorption coefficient and extinction coefficient as presented in Fig. 8 and the s_1g_1 GEF presented in Fig. 2a, the spectral emissivity of a homogeneous LI900 slab with a fiber volume fraction of 0.0677 and different thicknesses are computed and presented in Fig. 10. Note that a thickness of 1 cm is sufficient to reach the optically thick limit in the long wavelength region ($\lambda > 5~\mu$m). The spectral intensity radiated from a slab with thickness of 0.1 and 1 cm at different temperature is shown in Figs. 11a and 11b. Qualitatively, the optically thick case ($L = 1$ cm) at $T = 2000$ K in Fig. 11b agrees reasonably well the measured intensity presented in Fig. 9. Indeed, with the reformulation from a highly forward scattering medium to an isotropically scattering medium, one would not expect exact quantitative agreement on both the magnitude of the intensity and its overall wavelength dependence. Considering the relatively large uncertainty of the slab composition, the reported temperature and the measurement in general, the agreement is remarkable.
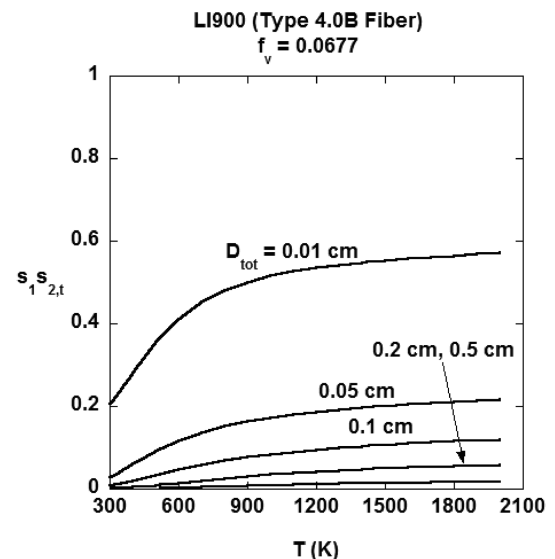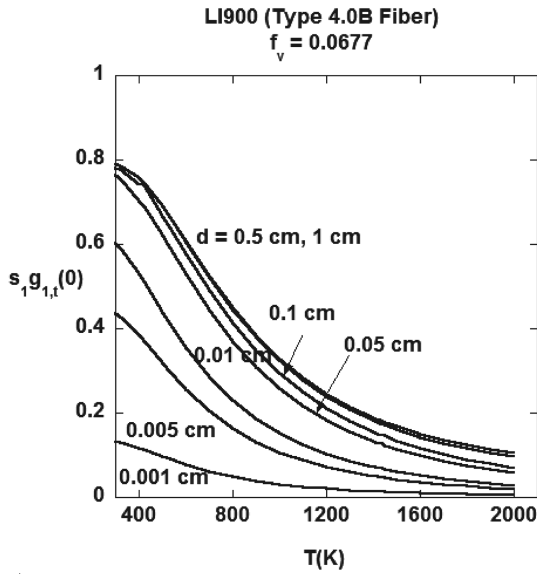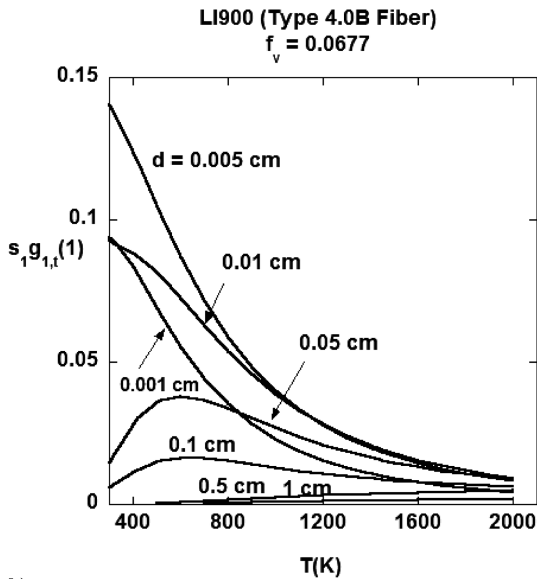
LI900 (Type 4.0B Fiber)
$f_v = 0.0677$

Fig. 13 The total exchange factor $s_1s_{2,t}$ as a function of temperature and total slab thickness.

LI900 (Type 4.0B Fiber)
$f_v = 0.0677$
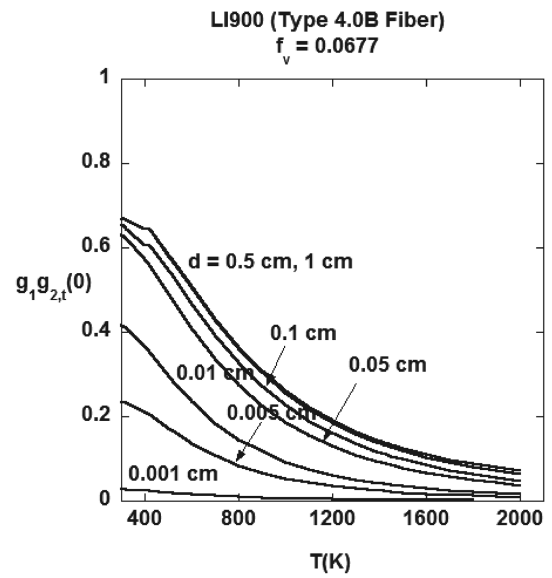

a)

LI900 (Type 4.0B Fiber)
$f_v = 0.0677$

b)

Fig. 14 a) The total exchange factor $s_1 g_{1,t}(0)$ as function of temperature and thickness of the volume element V_1. b) The total exchange factor $s_1 g_{1,t}(1)$ as a function of temperature and thickness of the volume element V_1.

LI900 (Type 4.0B Fiber)
$f_v = 0.0677$

a)

LI900 (Type 4.0B Fiber)
$f_v = 0.0677$

b)

Fig. 15 a) The total exchange factor $g_1 g_{2,t}(0)$ as a function of temperature and thickness of the volume element V_1 (the volume V_2 is assumed to have the same thickness). b) The total exchange factor $g_1 g_{2,t}(1)$ as a function of temperature and thickness of the volume element V_1 (the volume V_2 is assumed to have the same thickness).

It is also interesting to note that in the calculation [Fig. 11b] and confirmed by experimental measurement (Fig. 9), the emitted intensity in the short wavelength region from 1 to 5 μm contributes significantly to the overall emission of the slab. As shown in Fig. 8, this is a wavelength region in which the absorption coefficient is small and the scattering effect is large (the scattering albedo ω is greater than 0.99). An accurate simulation of the scattering effect, as generated by the zonal–GEF method, is required to predict the correct heat transfer.
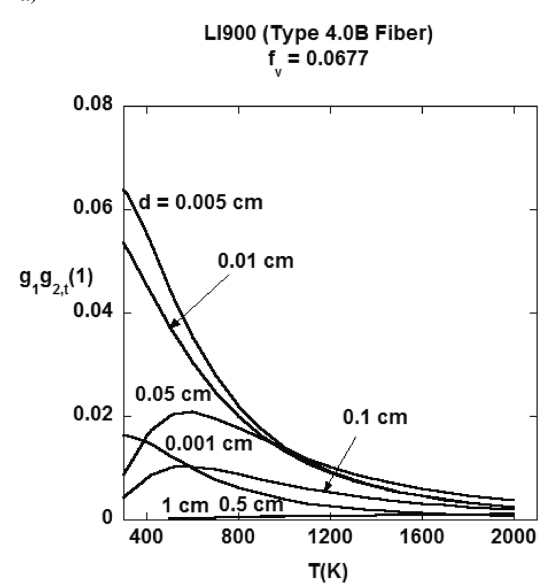
B. Effective Thermal Conductivity

Another set of data that were generated for this material is the effective thermal conductivity. Using a 2.54 cm thick sample, the effective thermal conductivity of LI900 was measured with a guarded-hot-plate apparatus [8].

Computationally, the heat transfer through the guarded-hot-plate apparatus can be simulated by a one-dimensional combined conduction radiation analysis. To simulate the total combined conductive and radiative heat transfer through the material, the four GEF's are first integrated over all wavelengths using the optical

properties shown in Fig. 8 to generate the total exchange factors. These factors are functions of the temperature of the emitting volume (or surface). The effect of surface temperature and thickness of the slab on the two surface-to-surface exchange factor is shown in Figs. 12 and 13. The volume to surface and volume to volume exchange factors are expressed in the form of $s_1 g_{1,t}(T, n)$ and $g_1 g_{2,t}(T, n)$ where T is the temperature of the emitting surface (volume) and n is the ratio the intervening distance to the thickness of the volume element ($n = D_L/d$ for $s_1 g_{1,t}$ and $n = D_m/d$ for $g_1 g_{2,t}$). Numerical data for $s_1 g_{1,t}(T, 0)$, $s_1 g_{1,t}(T, 1)$, $g_1 g_{2,t}(T, 0)$, and $g_1 g_{2,t}(T, 1)$ are presented in Figs. 14a, 14b, 15a, and 15b, respectively.

Physically, the two exchange factors, $s_1 s_{1,t}$ and $s_1 s_{2,t}$, can be interpreted as the total reflectivity and transmissivity of the slab, respectively. It is also interesting to note that since the material is practically purely scattering and nonabsorbing in the short wavelength region (see Fig. 8), it acts as a nonparticipating but highly attenuating medium at high temperature. Even for an optically thick slab ($d = 0.1$ cm), the transmissivity at high temperature

remains finite ($\sim$0.05). This effect is due almost entirely to scattering.

The two exchange factors, $s_1g_{1,t}(T,n)$ and $g_1g_{2,t}(T,n)$, have different behavior depending on the value of n. In Figs. 14a and 15a, $s_1g_{1,t}(0)$ and $g_1g_{2,t}(0)$ represent the total exchange factor between a volume element with an adjacent surface and volume, respectively. These two factors increase monotonically toward the optically thick limits as the thickness of the volume element (d) increases. The two factors also decrease monotonically as temperature increases because as temperature increases, the wavelength for dominant emission shifts to the shorter wavelength region which has a smaller absorption coefficient. In Figs. 14b and 15b, $s_1g_{1,t}(1)$ and $g_1g_{2,t}(1)$ represent the total exchange factor between a volume element with a surface and volume element with an intervening volume element of the same thickness d. As the thickness of the volume element increases, the exchange factors first increase due to increased absorption by the absorbing element, and then decrease due to the increased attenuation by the intervening element. Unlike $s_1s_{2,t}$, the exchange factors decrease to zero in the high temperature limit because these factors are proportional to the absorption coefficient which

approaches zero in the short wavelength region. Similar behavior are observed for other exchange factors, $s_1g_{1,t}(T,n)$ and $g_1g_{2,t}(T,n)$, with $n > 1$.

A combined conduction and radiation analysis of a 2.54 cm thick LI900 slab was conducted to simulate the effective conductivity measurement. A uniform grid size of 0.05 cm is used. The two boundaries are assumed to be black and maintained at constant temperatures with a temperature difference of 100 K between the two surfaces. A predicted effective thermal conductivity is generated from the predicted heat flux, Q, from the following relation

$$k_{\text{eff}} = \frac{QL}{\Delta T} \quad (1)$$

with L being the slab thickness (2.54 cm) and ΔT the temperature difference (100 K). A comparison between numerical prediction and measurements is shown in Fig. 16. The conductivity of a silica/air mixture at the volume fraction of 0.0677, which is used in the combined conductive radiative heat transfer calculation, is shown in the same figure for comparison. It can be readily observed that the combined conduction radiation analysis with GEF is generally effective in predicting the measured effective conductivity.

The discrepancy at higher temperature can be attributed to two factors. First, the conductivity of a silica fiber/air mixture presented in Fig. 16 and used in the calculation were computed using a homogeneous mixture, volume averaged model for the combined conductivity using the conductivity of solid silica fibers and air. The homogeneous model, however, tends to underpredict the mixture conductivity since the presence of air effectively increases the contact area between fibers, particularly for short fibers. The second factor is the uncertainty of the surface conditions of the two boundaries. As shown in Figs. 13, 14a, 14b, 15a, and 15b, LI900 is highly reflective and nonabsorbing in regions with high temperature. A slightly reflective bounding surface can lead to a significant change in the predicted heat transfer and therefore a significant change in the predicted effective thermal conductivity.
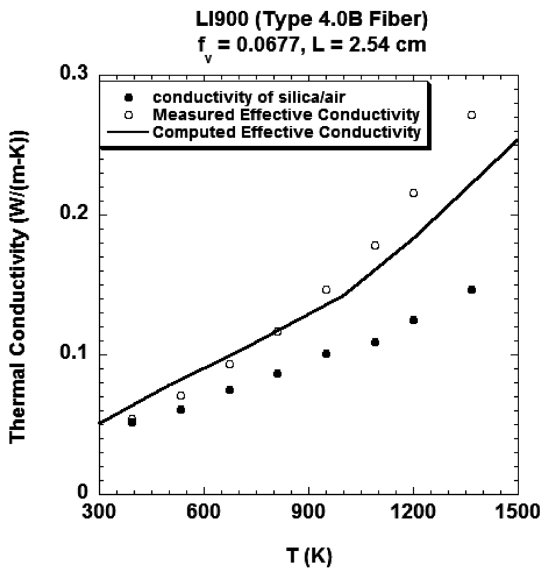

Fig. 16 Comparison between the predicted and measured effective thermal conductivity for LI900. The thermal conductivity of a silica fiber/air mixture with a volume fraction of 0.0677 is also shown.
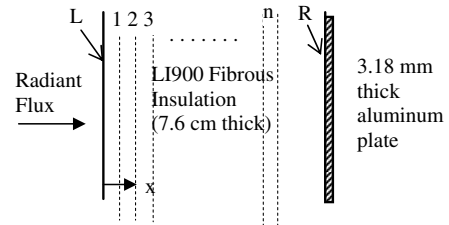

Fig. 18 Experimental setup and coordinate system, the broken line represents the zonal elements used in the zonal–GEF analysis. L and R are identification of the wall at $x = 0$ and $x = 7.6$ cm, respectively.
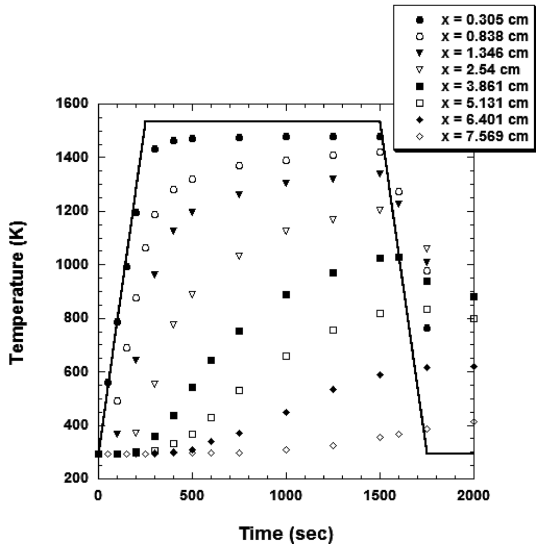

Fig. 17 Transient temperature response of a LI900 (4.0 B) tile heated by radiant heat flux. (The solid line is the temperature imposed at the boundary $x = 0$ by the incident radiant flux).
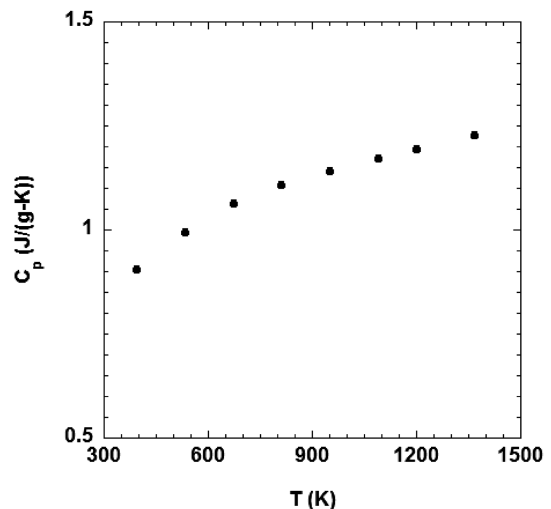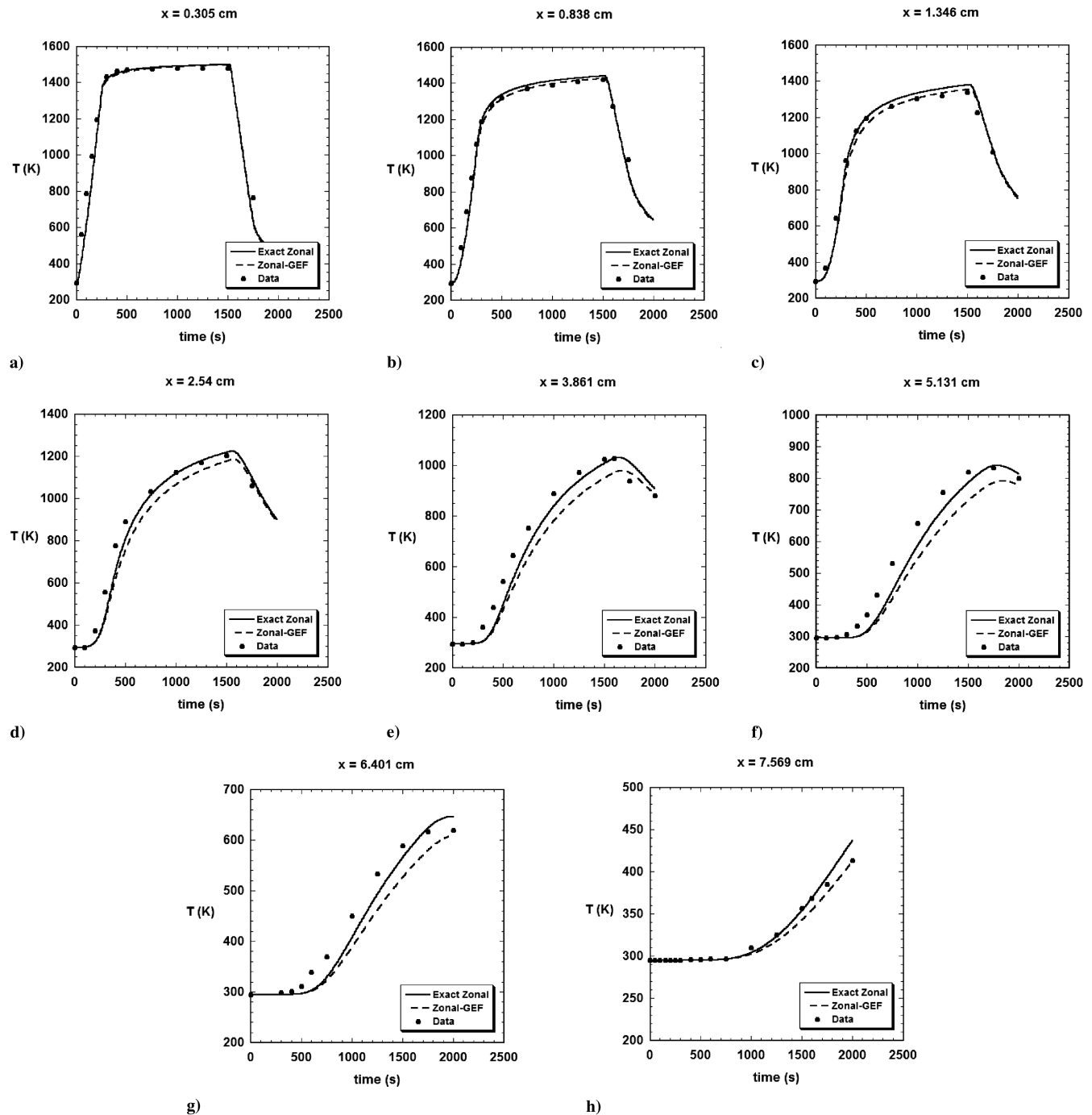

Fig. 19 Specific heat of the LI900 fibrous composite used in the transient calculation.

Fig. 20 a) Comparison between the predicted and measured temperature at $x = 0.305$ cm. b) Comparison between the predicted and measured temperature at $x = 0.838$ cm. c) Comparison between the predicted and measured temperature at $x = 1.346$ cm. d) Comparison between the predicted and measured temperature at $x = 2.54$ cm. e) Comparison between the predicted and measured temperature at $x = 3.861$ cm. f) Comparison between the predicted and measured temperature at $x = 5.131$ cm. g) Comparison between the predicted and measured temperature at $x = 6.401$ cm. h) Comparison between the predicted and measured temperature at $x = 7.569$ cm.

C. Transient Heating of a LI900 Slab

A third set of experimental data for this material were generated by heating a sample with a time varying surface heat flux in a quartz lamb radiant heating facility [8]. A detailed description of the experiment is given elsewhere [6,8] and will not be repeated here. Specifically, a 0.15 m square LI900 slab with a thickness of 7.6 cm thickness was heated. Thermocouples are installed in the interior of the slab to measure the interior temperature. The radiant heating rate was automatically adjusted to follow a programmed surface temperature versus time which was to raise the surface temperature from a nominal 295 to 1533 K in 250 s. The surface temperature was then held at 1533 K for 1250 s. The radiant heat flux was then terminated and the surface temperature dropped linearly to the ambient temperature (295 K) in another 250 s. The surface temperature profile and the measured interior temperature for one specific test are shown in Fig. 17. A schematic of the experimental setup and the coordinate system used in the analysis are shown in Fig. 18. The instrumented specimen was bonded with RTV adhesive to a 3.18 mm thick aluminum plate. This is included in the numerical model as shown in Fig. 18. The maximum estimated uncertainty in the temperature measurement was ±15 K.

The mathematical formulation of a combined conduction radiation numerical solution to this problem with the full zonal method (i.e., the exchange factors are calculated exactly without using the approximate GEF) has been presented elsewhere and will not be repeated here. The density of the fibrous composite used in the

calculation is taken to be 0.149 gm/cm³, the volume average between silica and air (at the volume fraction of 0.667). The specific heat for the composite is assumed to be that of silica and is shown in Fig. 19. The boundary surfaces are assumed to be black. Using the GEF's as presented in Figs. 12–14 and 15b [including the GEF $s_1 g_{1,t}(T, n)$ and $g_1 g_{2,t}(T, n)$ with higher order of $n > 2$], a new set of solution is generated and the temperature predictions are compared with the experimental data, as well as the more exact numerical solution in Figs. 20a–20h.

In general, the zonal–GEF approach predicts a slightly lower temperature than the exact zonal approach. But both methods yield solutions that compare well with experimental data. In view of the uncertainty of the experiment (e.g., the location of the thermocouples and its error, the uncertainty of boundary condition in the back of the aluminum plate), this agreement is quite satisfactory and it verifies the general accuracy of the zonal–GEF approach.

IV. Conclusions

The zonal–GEF method is demonstrated to be an accurate and efficient approach to analyze the radiative heat transfer in highly scattering materials. For the LI900 fibrous insulation tiles with 4.0 μm silica fibers, the method is effective in generating predictions that correlate well with three separate set of experimental data, spectral intensity, effective thermal conductivity and transient response of a slab under radiant heating.

Radiatively, the LI900 fibrous insulation material is shown to be an effectively pure scattering material in the short wavelength region ($\lambda < 5$ μm). The material is strongly attenuating, but nonabsorbing to high temperature radiation. Even if the material appears to be optically thick, the thermal radiation effect is nonlocalized and finite energy exchange can occur over distances in the range of millimeter. A nonlocalized radiation model (such as the zonal–GEF method) is thus needed for any detailed numerical thermal performance analyses for this class of materials.

References

[1] Cunnington, G. R., and Lee, S. C., "Radiative Properties of Fibrous Thermal Insulation," *Journal of Thermophysics and Heat Transfer*, Vol. 10, No. 3, 1996, pp. 460–466.

[2] Siegel, R., and Howell, J. R., *Radiative Heat Transfer*, 4th ed., Taylor–Francis, New York, 2002.

[3] Lee, S. C., and Cunnington, G. R., "Theoretical Models for Radiative Transfer in Fibrous Media," *Annual Review of Heat Transfer*, Vol. 9, 1998, pp. 159–218.

[4] Yuen, W. W., and Takara, E. E., "The Zonal Method: A Practical Solution Method for Radiative Transfer in Non-Isothermal Inhomogeneous Medium," *Annual Review of Heat Transfer*, Vol. 8, 1997, pp. 153–215.

[5] Yuen, W. W., "The Multiple Absorption Coefficient Zonal Method (MACZM): An Efficient Computational Approach for the Analysis of Radiative Heat Transfer in Multi-Dimensional, Inhomogeneous and Non-Gray Media," *Numerical Heat Transfer* (to be published).

[6] Yuen, W. W., Takara, E., and Cunnington, G. R., "Combined Conductive/Radiative Heat Transfer in High Porosity Fibrous Insulation Materials: Theory and Experiment," *Proceedings of the 6th ASME–JSME Joint Thermophysics Conference*, 2003, p. 201.

[7] Joseph, J. H., Wiscombe, W. J., and Weinman, J. A., "The Delta-Eddington Approximation for Radiative Heat Transfer," *Journal of the Atmospheric Sciences*, Vol. 33, No. 12, 1976, pp. 2452–2459.

[8] Banas, R. P., and Cunnington, G. R., "Determination of the Effective Thermal Conductivity of the Space Shuttle Orbiter's Reusable Surface Insulation (RSI)," AIAA Paper 74-730, 1974.

[9] Lee, S. C., and Cunnington, G. R., "Conduction and Radiation Heat Transfer in High-Porosity Fiber Thermal Insulation," *Journal of Thermophysics and Heat Transfer*, Vol. 14, No. 2, 2000, pp. 121–136.